ACS APPLIED BIO MATERIALS

www.acsabm.org Article

PtNPt/MWCNT-PEDOT:PSS-Modified Microelectrode Arrays for the Synchronous Dopamine and Neural Spike Detection in Rat Models of Sleep Deprivation

Zeying Lu, Shengwei Xu, Hao Wang, Enhui He, Juntao Liu, Yuchuan Dai, Jingyu Xie, Yilin Song, Yun Wang, Yiding Wang, Lina Qu,* and Xinxia Cai*

Cite This: ACS Appl. Bio Mater. 2021, 4, 4872−4884 Read Online

ABSTRACT: In this study, a biosensor assembly based on microelectrode arrays (MEAs) modified with PtNPt/MWCNT-PEDOT:PSS nanocomposites is presented to synchronously detect the dopamine (DA) and electrophysiological activities in rat brains. Different morphological and electrochemical characterizations were conducted to show the excellent mechanical and electrical properties of the as-prepared probes. The developed biosensors realized the sensitive and selective detection of DA with the existence of significant interferences such as uric acid (UA), ascorbic acid (AA), glutamate (Glu), and 3,4-dihydroxyphenyl-acetic acid (DOPAC). Calibration curve for the DA response was linear with the concentration from 0.05 μM to 79 μM (R = 0.999), with a sensitivity of 30.561 pA/μM and detection limit as low as 50 nM. Finally, the proposed microelectrode was applied to be implanted into the cortex and caudate putamen (CPU) of rats, which was demonstrated to stably measure the synchronous neurochemical and neurophysiological changes caused by 72 h sleep deprivation. The in vivo measuring results showed that the sleep deprivation increased the DA release and neural spike activity in both cortex and CPU. The local field potential (LFP) power in the delta and theta band was significantly increased as well. These changes in brain may reflect the brain's adaptive reaction toward the side effects induced by sleep deprivation and may partially explain the mechanism of forced wakefulness in the presence of accumulated sleep pressure.

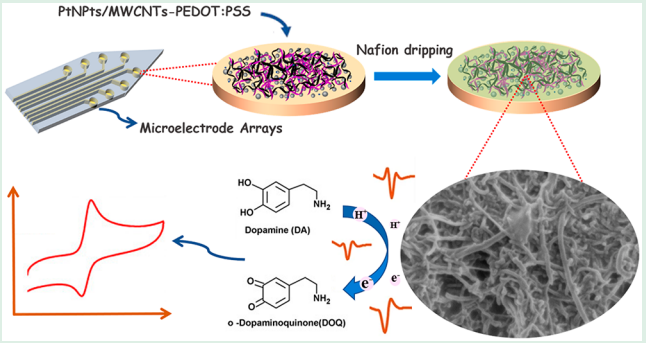

KEYWORDS: *MEA, sleep deprivation, dopamine, MWCNTs, PEDOT, spike, LFP*

INTRODUCTION

Maintaining a regular sleep−wake cycle is profound across species. Typically, both sleep and wakefulness are controlled by a network of the brain nucleus, which integrates circadian and homeostatic regulations and interacts in a complex fashion.[1] Disruption of this cycle will bring about various adverse consequences and threaten an individual's daily performance and health.[2,3] The public health effects of sleep deprivation (SD) are immense and could induce a variety of physiological changes, which are associated with risks for various medical conditions, such as diabetes, weight loss, hypothermia and impaired immune functions.[4−6] Multiple experimental data indicated a role for the prefrontal cortex in mediating normal sleep physiology, dreaming, and sleep-deprivation phenomena.[7,8] It is widely known that the caudate putamen (CPU), which resides in the forebrain, is involved in various physiological processes including motor control, habit formation, and waking-related behaviors.[9] However, studies about their roles in sleep−wake regulation have been limited. More studies are needed to better understand the underlying mechanism of sleep and reflect the impaired brain functions induced by SD and accurately monitor the neural activities in the cortex and CPU at the cellular level.

Neuropharmacological experiments have found that the variations in brain levels of certain neurotransmitters are involved in sleep−wake cycle control.[10,11] Dopamine is involved in a variety of behavioral and psychological processes, including motor activities, concentration, motivation, and reward, and all of these functions operate on the basis of wakefulness.[12−15] There is increasing evidence that dopamine (DA) could modulate wakefulness and exert a wake-promoting effect,[16−18] as wake-promoting medications could increase the release of brain DA.[19] Furthermore, patients with Parkinson's disease who endure a progressive depletion of DA have been reported to

Received: February 9, 2021
Accepted: April 7, 2021
Published: May 15, 2021

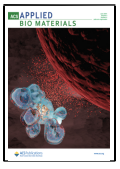

https://doi.org/10.1021/acsabm.1c00172
ACS Appl. Bio Mater. 2021, 4, 4872−4884

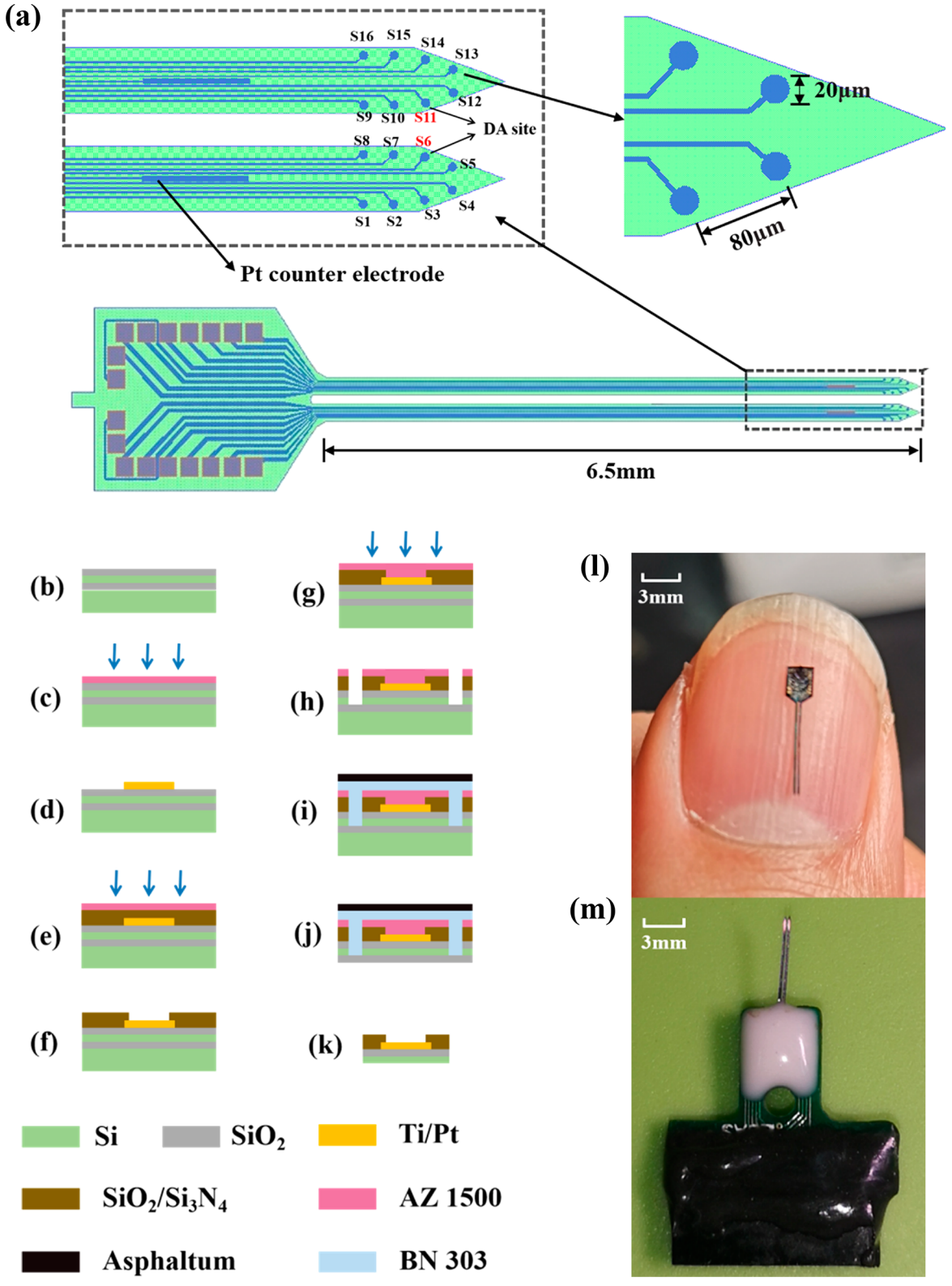

Figure 1. Design and fabrication of the implanted microelectrode. (a) Two-shank MEA structure. The MEA contains two DA recording sites and 14 neurophysiology recording sites. (b) Implantable microelectrode array (MEA) is fabricated using silicon-on-insulator (SOI) substrates through the microelectromechanical systems (MEMS) method. (b–k) Standard MEMS photolithography steps performed in our super clean laboratory. (l) Completed MEA placed on a fingernail. (m) MEA connected to a printed circuit board.

suffer from severe sleep disorders including narcolepsy, insomnia, sleep apnea, and restless legs syndrome.[20] Also, mutations in the gene encoding for the dopamine transporter in the fly could substantially decrease sleep.[21] Thus, on the basis of the effect of dopamine on the maintenance of wakefulness, it is of importance to investigate the impacts of sleep deprivation on DA activity as well as its modulating effect on the sleep–wake circle.

https://doi.org/10.1021/acsabm.1c00172
ACS Appl. Bio Mater. 2021, 4, 4872–4884

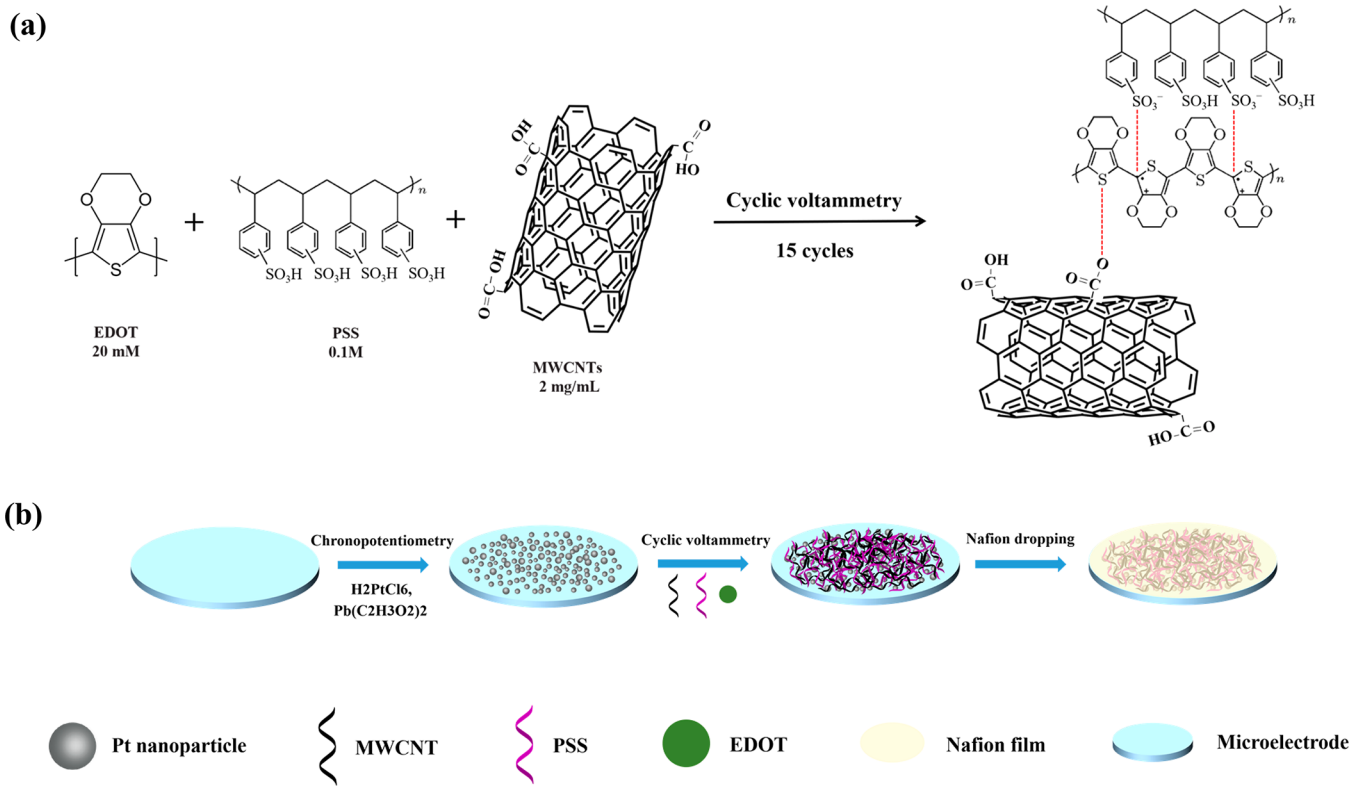

Figure 2. Modification process of the microelectrode. (a) Combination mechanism of MWCNTs, PEDOT, and PSS. (b) Scheme for electrochemical deposition of PtNPt/MWCNT-PEDOT:PSS onto the microelectrodes.

Because of the technological limitations, most researchers have focused only on single-mode recording of single-unit activities or neurotransmitter release. The sampling techniques such as capillary electrophoresis and capillary liquid chromatography have become well-established for monitoring low-molecular-weight neurotransmitters.[22] Even though these methods have realized the measurements of various neurotransmitters and chemicals with high selectivity and sensitivity, its poor spatial and temporal resolution have limited its application for studying behavior and small brain nuclei.[23] Neural spike activities have been studied mainly by metal electrodes and glass micropipettes. These types of electrode can be easily fabricated but their imprecise size and spacing have resulted in a low reproducibility.[24] Therefore, development of the detection method that possesses a high spatial resolution and could perform simultaneous DA and neuronal activity measurement is essential to investigating neural activity changes after sleep deprivation.

Nanomaterials have a catalytic effect on the oxidation of multiple neurochemicals, and several researchers have reported the excellent performance of the nanocoated electronic sensors.[25] To realize the improved detection ability of MEAs, the surface of microelectrodes has been modified with metal nanoparticles, such as nanogold and Pt-black nanoparticles.[26] The Pt nanoparticles (PtNPts) possess superior catalytic ability toward various electroactive molecules such as DA, which could significantly improve the electron tunneling efficiency between the interface of electrode and reagent.[27] Besides, conductive polymers of various types have been extensively used in the development of biosensors.[28] Among them, poly(3,4-ethylenedioxythiophene) and polystyrenesulfonate (PEDOT:PSS) polymer has been attracting more and more attention based on its extraordinary characteristics such as enhanced electrical conductivity, electrical stability, water solubility and homogeneous film growth on semiconducting electrodes.[29,30] Besides, the multiwalled carbon nanotubes (MWCNTs) have been widely reported to own excellent chemical and electrical properties, including extraordinary conductivity, elevated electrochemical reactions rate, and enlarged surface area, as well as high durability.[31] Therefore, the further incorporation of PtNPts, MWCNTs and PEDOT:PSS would not only decrease the impedance and enhance the electron transmission but also improve the affinity of the composite film.

As a high-resolution and high sensitivity tool for neuronal research, the microelectrode arrays (MEAs) have been promoted by the recent advances in microelectromechanical system (MEMS) technology. Unlike the traditional electrophysiological method such as EEG or ECOG, the MEA is extremely small in size and can be implanted into the brain of the animal to directly record the neuronal activities. In addition, the MEA can realize the recording of neurons at multiple electrode sites simultaneously, which can obtain more information from a single test. In this work, we designed and mass fabricated a two-shank microelectrode array (MEA) for the simultaneous detection of DA concentration and neuronal activities in the cortex and CPU of rats before and after sleep deprivation. All recording sites were modified with PtNPt/MWCNT-PEDOT:PSS nanocomposites to promote electron transmission. The Nafion film was specially modified on the DA detection site to further eliminate the effect of other interferences. The electrocatalytic activity, selectivity, and performance of the designed biosensor was evaluated, which verified its stable and precise measurement capacity. The in vivo studies demonstrated the abilities of the modified MEA to stably record the DA and

https://doi.org/10.1021/acsabm.1c00172
ACS Appl. Bio Mater. 2021, 4, 4872−4884

electrophysiology changes in certain nuclei of rat brain. The neurochemical and neurophysiological activity changes we detected could partially reflect the adverse effects brought by sleep deprivation.

MATERIALS AND METHODS

Reagents and Apparatus. 3,4-Ethylenedioxythiophene (EDOT) was obtained from Aladdin, China. Polystyrenesulfonate (PSS) was purchased from HEROCHEM, China. Multiwalled carbon nanotubes (MWCNTs) were obtained from XFNANO, China. 4-Chloro-DL-phenylalanine (PCPA), phosphate-buffered saline (PBS), dopamine, and other chemicals were supplied by Sigma-Aldrich, China.

The 128-channel neural data recording system (Blackrock Microsystems, USA) was used to detect the neural signal. The Gamry electrochemical workstation (Gamry Reference 600, Gamry Instruments, USA) was used to perform the electrochemical measurements. Animal anesthesia during the experiments was performed by the animal isoflurane anesthesia machine (R580S, RWD Life Science, China). A micropositioner (model 2662, David LOPF instrument, USA) was used to push the implantable MEAs into the target region. Optical and scanning electron microscopy (SEM, S-4800, Hitachi, Japan) were used to characterize the surface morphology of the modified microelectrode. Other apparatuses included a high-speed drill (carbon burr drill bits, 0.7 mm, SAESHIN Ltd., Daegu, Korea) and a stereotaxic frame (Stenting, Wood Dale, IL, USA).

MEA Design and Fabrication. The electrodes used for recording are designed with shanks that have a length of 6.5 mm for the penetration into the rat brain, and this length of shank could detect the signals in cortex as well as CPU. As shown in Figure 1a, the MEA silicon probe consists of two shanks and there is a u-shaped array of eight round microelectrode sites (20 μm in diameter) on the tip of each shank. Two rectangular Pt counter electrodes were also integrated on the MEA. As shown in Figure S1, when MEA was applied in signal detection, sites 6 and 11 on the MEA were connected to the neurochemical module of the recording device and used as DA recording channels, whereas the other sites were connected to the electrophysiological module of the recording device and were used as electrical recording channels.

The MEAs were mass fabricated by MEMS thin-film technology in the superclean room, which followed the process as described in our previous studies:[32,33] (1) The insulator layer of SiO_2 (500 nm) was grown onto the wafer through thermal oxidation (Figure 1b). (2) Ti/Pt (30 nm/250 nm) was sputtered and patterned through the lift-off process, which formed the conducting layer on the electrode (Figure 1c, d). (3) The passivation layer of SiO_2/Si_3N_4 (300 nm/500 nm) was deposited through plasma-enhanced chemical vapor deposition (PECVD) and then selectively removed with a resist mask through SF6 reactive ion etching to expose the microelectrode sites and the bonding pads (Figure 1e, f). (4) The top silicon layer (30 μm) was selectively etched down to the buried oxide layer with a resist mask using inductively coupled plasma reactive ion etching (ICP-RIE) (Figure 1g, h). (5) The wafer was covered with the melting asphaltum to protect the top side of the silicon (Figure 1i). (6) The back side of the silicon was wet etched in a KOH solution (50%, 80 °C) until it stopped automatically, and then the buried oxide layer (2 μm) was removed in the solution of HF buffer (Figure 1j). (7) The wafer was placed in the developing liquid to dissolve the top side of the asphaltum and release the probes (Figure 1k). Figure 1l showed that the completed MEA was placed on the fingernail. The probes were then assembled onto interfacing printed circuit boards via wire bonding and got coated in silicone rubber, as shown in Figure 1m.

Modification of PtNPt/MWCNT-PEDOT:PSS Nanocomposites. Nanomaterials are modified to promote the electron transfer capabilities. In this work, the mixture of Pt nanoparticles and MWCNTs-PEDOT:PSS nanocomposites were applied to improve the performance of microelectrode. Figure 2a illustrated the combination mechanism of MWCNTs, PEDOT and PSS. During the electrochemical deposition process, the monomer EDOT in the solution was first oxidized into free cation radicals EDOT+, and then the EDOT+ formed conjugated PEDOT chains through polymerization. The conjugated PEDOT chains could react with free π electrons on the wall of the MWCNTs to form $\pi-\pi$ conjugation, which allowed PEDOT to grow uniformly on the surface of MWCNTs and together being deposited onto the surface of microelectrode. In consequence, MWCNTs have been brought to the electrode surface with the assistance of growing PEDOT polymer chains, forming a high-performance nanocomposite film. Based on this architecture, the hybrid nanocomposite film owns the property of good conductivity, high charge transfer, and high porosity, which makes it a promising electrochemical biosensor.

A three-electrode setup was used in the modification process (Pt wire as the counter electrode; AglAgCl as the reference electrode; MEA electrodes as the working electrode). As shown in Figure 2b, the PtNPts layer were first electrodeposited onto the round recording site with chronoamperometry (CA, − 1.1 V, 50 s), in the plating solution involving 48 mM chloroplatinic acid and 4.2 mM lead acetate with a 1:1 mixture. Then, the electrodeposition of MWCNT-PEDOT:PSS was performed by cyclic voltammetry sweeping (0−0.95 V) for 15 cycles in the mixture solution of PSS (0.1 M), EDOT (20 mM), and MWCNTs (2 mg/mL). Finally, the ion-exchange resin Nafion (1% in ethanol) was dripped via micropump onto the DA measuring channel under the microscope and then dried at 100 °C for 20 min.

Sleep Deprivation of Rats. Six male Sprague−Dawley rats (200−250 g) were prepared in the experiments and were allowed unrestricted access to food and water. The air-conditioned experimental animal room was kept at the temperature of 21∼23 °C, with a natural light−dark cycle (light was on from 9:00 A.M. to 9:00 P.M.). All animal care protocol was under the guide of institutional Animal Ethics Committee.

Sleep deprivation model in rats was induced by the chemical reagent method. *p*-Chlorophenylalanine (PCPA) was used in this study, which is the inhibitor of serotonin (5-HT) synthesis and could induce a long-lasting sleep loss on the animals.[34,35] PCPA was suspended evenly in a gum acacia (wt, 0.5%)/physiological saline solution (pH 7.5). The rats were given an intraperitoneal injection of PCPA suspension (300 mg/kg) daily for two consecutive days. After the injection of PCPA, the rats started to lose the circadian rhythm and maintained sleeplessness all the time, which verified the successful establishment of the model.

Animal Surgery and Data Acquisition. All animal experiments were conducted in a professional biological laboratory and the surgeries were conducted under the Guide for the Care and Use of Laboratory Animals. The animal surgery and signal detection were performed 72 h before and after the injection of PCPA suspension. During the surgery process, animals were immobilized in the stereotaxic frame and anesthetized by isoflurane anesthesia. As shown in Figure S2a, b, MEAs were vertically implanted to the right lateral cortex and CPU in sequence (position coordinate, ML, 2.4 mm; AP, 0.96 mm; DV, −1.5 mm/−3.8 mm). Two more sites were drilled over the prefrontal cortex surface to place the AglAgCl reference electrode and a screw ground electrode.

All the recording processes were performed under the anesthesia of the rats. For the prevention of external electromagnetic interference, the stereotaxic frame with the rat was put into a grounded, shielded box during the measurements. The implanted MEAs were connected to a 128-channel electrophysiological data acquisition system to detect the neural activity. The sample rate for the electrophysiological signals is 30 kHz. The spike firing was obtained from a high pass filter (250 Hz), and the local field potential were obtained from a low pass filter (250 Hz).

After the experiments, the brain was dehydrated and sectioned, and the wound trace was marked by the red rectangular as shown in Figure S2c, verifying that the electrode implantation position was exactly the predetermined position.

RESULTS AND DISCUSSION

Growth of MWCNTs-PEDOT:PSS Film. The conducting materials were deposited onto the electrode surface via electrodeposition method, which could realize the control of morphology and thickness. And the electrodeposition was performed under the aqueous environment at a moderate pH

https://doi.org/10.1021/acsabm.1c00172
ACS Appl. Bio Mater. 2021, 4, 4872−4884

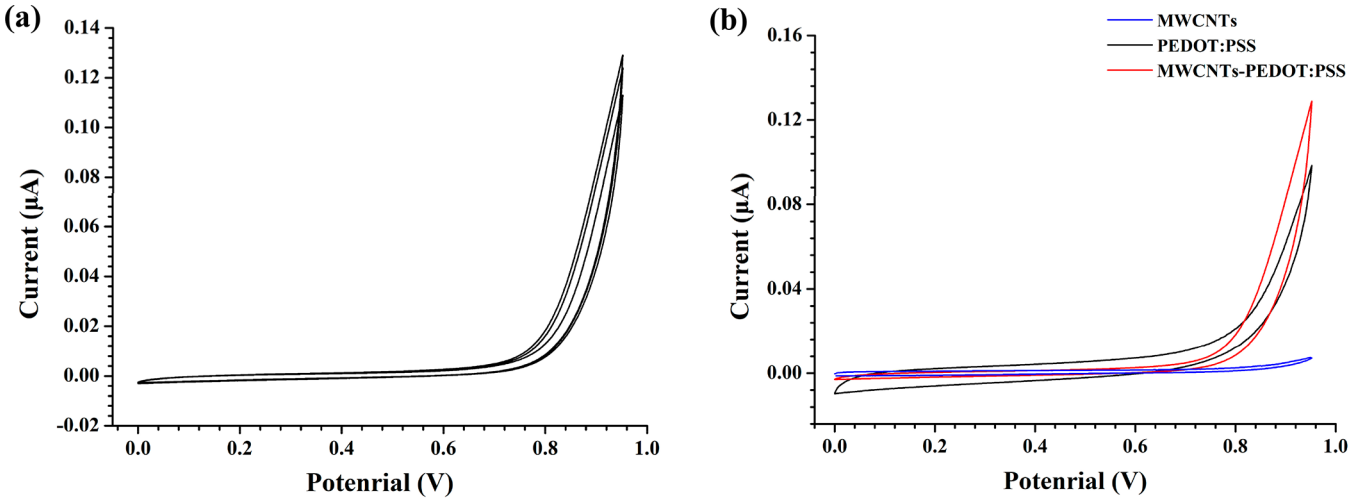

Figure 3. Growth of MWCNT-PEDOT:PSS composite film onto the microelectrode. (a) Cyclic voltammograms recorded during electrodeposition of MWCNTs-PEDOT:PSS onto microelectrode. (b) Comparison of cyclic voltammograms scans during the electrodeposition with MWCNTs, PEDOT:PSS, and MWCNT-PEDOT:PSS.

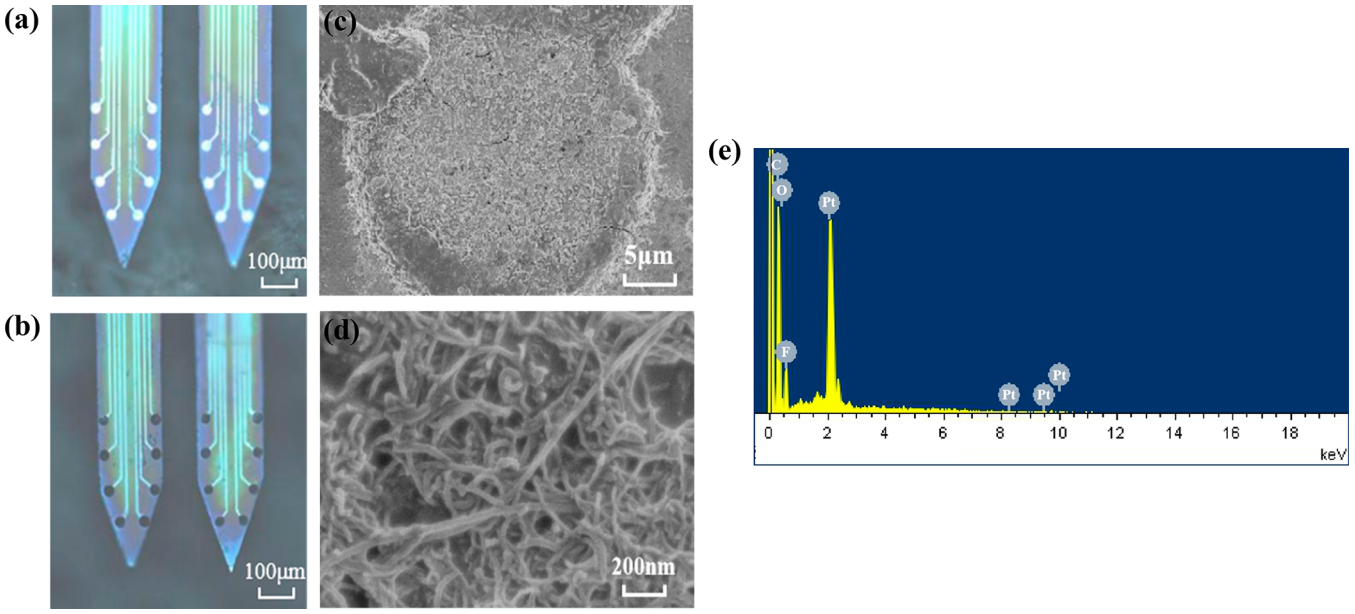

Figure 4. Morphology and structural characteristics of the MEA. Optical microscope images of the microelectrode (a) before and (b) after the electrodeposition of PtNPt/MWCNT-PEDOT:PSS nanocomposite. (c) Scanning electron microscope (SEM, 3.5k) images of the electrode modified with PtNPt/MWCNT-PEDOT:PSS nanocomposite. (d) Enlarged scanning electron microscope (SEM, 70k) images of the electrode modified with PtNPt/MWCNT-PEDOT:PSS. (e) EDX spectrum of the PtNPt/MWCNT-PEDOT:PSS nanocomposite.

and ambient temperature. No toxic oxidants, surfactants, reductants, or electrolytes were used during this process.

During the growth of MWCNTs-PEDOT:PSS film, the recorded cyclic voltammetry (CV) showed an oxidation peak at +950 mV, which was the typical characteristic for PEDOT polymerization (Figure 3a). The intensities of the oxidation peaks current increased gradually with each scan, indicating the deposition process of conducting polymers. As shown in Figure 3b, once the carbon tubes or PEDOT:PSS were removed from the deposition solution, much lower intensities of these peak current could be observed, which further verified the polymerization of PEDOT and coexistence of MWCNTs in the grown film.

Morphological and Structural Analyses. The morphological and structural features of PtNPt/MWCNT-PEDOT:PSS modified microelectrode were characterized by optical microscope and SEM measurements. The optical image showed that the nanocomposite film was successfully electrodeposited onto the electrode with a black surface (Figure 4a, b). The micrograph of SEM showed a relatively rough and porous surface of the electrode site after modification with PtNPt/MWCNT-PEDOT:PSS (Figure 4c, d). The observed wrinkled and porous structure of the deposited film significantly enhanced the surface area and improved the conductivity of the electrode. As shown in Figure 4e, the energy-dispersive X-ray (EDX) spectrum of SEM displayed that the typical metallic element is "Pt", indicating the distribution of PtNPts in PtNPt/MWCNT-PEDOT:PSS nanocomposite. And the element "F" was typically found in Nafion, so the existence of "F" showed

https://doi.org/10.1021/acsabm.1c00172
ACS Appl. Bio Mater. 2021, 4, 4872−4884

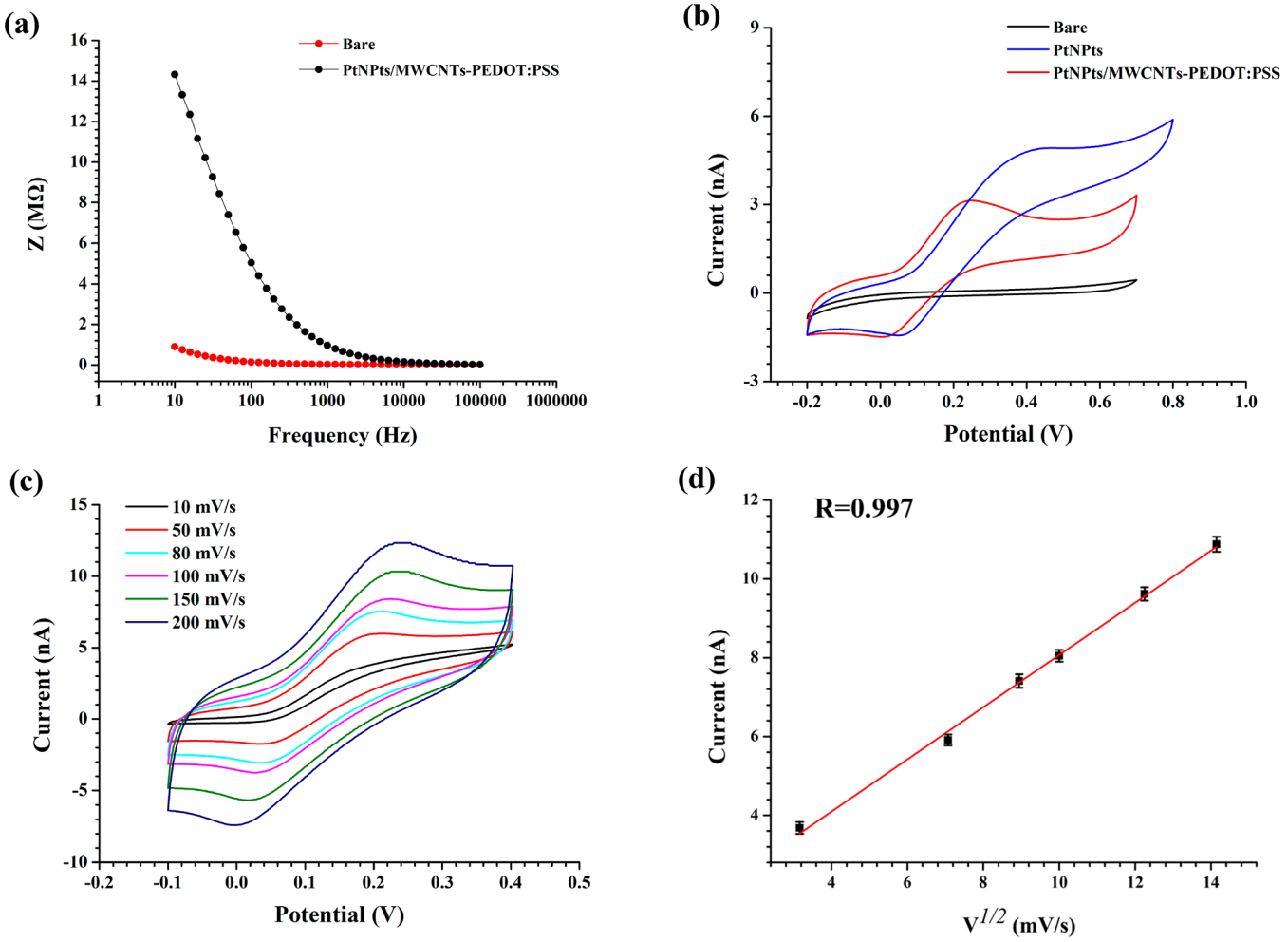

Figure 5. Electrochemical characterization PtNPt/MWCNT-PEDOT:PSS-modified electrode. (a) Bode plot (impedance−frequency plot) comparison of the impedance Z values with one bare electrode and one modified electrode. (b) Cyclic voltammograms of the bare and modified electrode in 100 μM DA. (c) Cyclic voltammograms of the modified electrode measured in 200 μM DA with different scan rate (0.01−0.2 V/s). (d) Fitting plot of the square root of the scan rate ($v^{1/2}$) and the oxidation peak current.

that the microelectrode surface had been successfully coated with Nafion.

Electrochemical Characterization of PtNPt/MWCNT-PEDOT:PSS-Modified Electrode. Electrochemical impedance spectroscopy (EIS) is a highly sensitive technique used to characterize the electrical properties of nanomaterials and their interfaces.[36] Impedance spectra of the bare and PtNPt/MWCNT-PEDOT:PSS modified microelectrodes were investigated in a PBS solution at pH 7.4. As shown in Figure 5a, with the sweeping frequency from 10 Hz to 0.1 MHz, the impedance of the electrodes under frequency changes of the AC signal was recorded. The impedances of two different electrode surfaces were compared at the frequency of 1 kHz. At 1 kHz, the impedance value for bare Pt electrode was about 964.25 kΩ, whereas the impedance value for PtNPt/MWCNT-PEDOT:PSS electrode was about 32.46 kΩ. The magnitude of electrode impedance was reduced by a factor of about 30 at 1 kHz.

Cyclic voltammetry (CV) measurement was conducted to evaluate the electron transmission abilities of the electrodes by measuring the redox peak potential of the sweeping curve. CV was performed in a DA solution of 100 μM using the bare, PtNPts, and PtNPt/MWCNT-PEDOT:PSS modified electrodes. Pairs of redox peaks corresponding each electrode were shown in Figure 5b. It can be seen that the bare electrode exhibited no obvious oxidation peak potential and showed weak current response to DA, indicating its incompetence to catalyze the DA reaction, whereas the oxidation peak potential was calculated as 200 mV for the PtNPt/MWCNT-PEDOT:PSS modified electrode, which is much lower than that of the PtNPt-modified electrode (400 mV). Compared with the previously reported DA sensors, the oxidation peak potential of our proposed DA sensor is also much lower.[37−39] The possible reason for the reduced oxidation potential may be attributed to the fact that the proposed PtNPt/MWCNT-PEDOT:PSS composites effectively facilitated the fast transfer of electrons between the electrode substrate and modified layer. To some extent, the reduction in oxidation potential is important, because it could effectively block various interferences to ensure the precision of DA measurement. Figure 5c represented the CV behavior of PtNPt/MWCNT-PEDOT:PSS-modified electrode in 200 μM DA solution at different scan rates (10−200 mV/s). It was clearly observed that the anodic and cathodic peak currents increased linearly with the increase of scan rate. As shown in Figure 5d, the oxidation peak current shows a linear relationship (R = 0.997) with the square root of the scan rate ($v^{1/2}$), which indicated a diffusion-controlled mass transfer phenomenon at the solution−electrode interface.

https://doi.org/10.1021/acsabm.1c00172
ACS Appl. Bio Mater. 2021, 4, 4872−4884

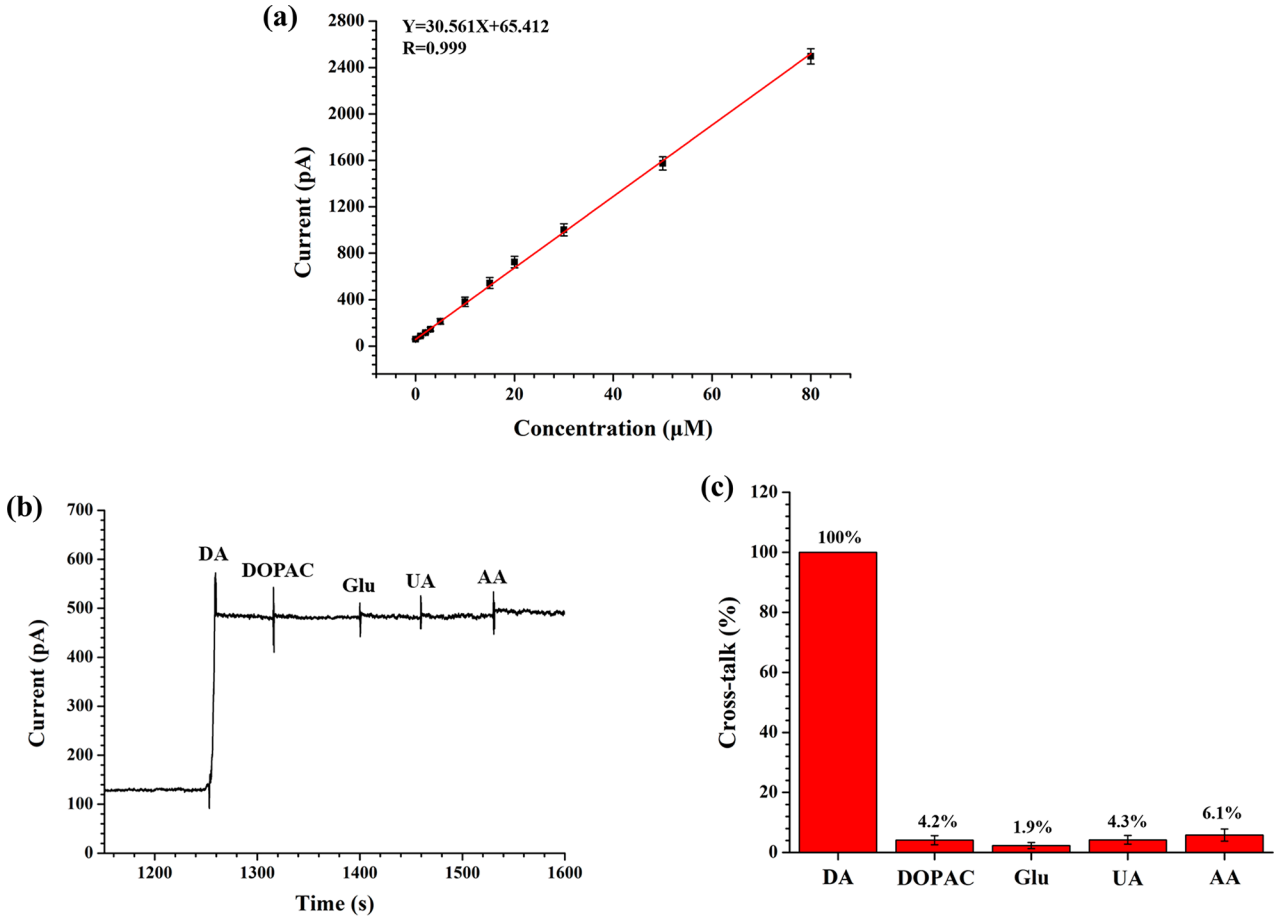

Figure 6. Amperometry measurements of DA electrodes. (a) Fitting plot of the relationship between the measured current and concentration. (b) DA electrode response to the addition of interfering materials (DOPAC, Glu, UA, AA) with a concentration of 20 μM. (c) Current response comparison between the interfering substances and DA.

Table 1. Comparison of the Proposed PtNPt/MWCNt-PEDOT:PSS-Modified Electrochemical Biosensors with Other Literature

electrode materials	method	detection limit (μM)	linear range (μM)	interferences	ref
PPy/sulfonated β-cyclodextrin	CV	3.2	10−40	AA	40
Au−Cu_2O/rGO	DPV	3.9	10−90	UA	41
CNT-N	DPV	1	1−20	AA	42
GNSs/CTAB	DPV, CV	0.6	4−52	glucose, UA, AA	43
PEDOT-COOH	DPV	0.15	1−85	UA, AA	44
PDA@CNT-PEDOT	DPV	0.62	2.2−10^6	AA, UA, Tryp	45
Pd/RGO/PEDOT	DPV	0.14	1−200	norepinephrine, epinephrine, UA, AA	46
PEDOT-LSG	DPV	0.33	1−150	AA, UA	47
PEDOT-Au NPs	CA	0.2	6−13000	AA, UA	48
PtNPt/MWCNt-PEDOT:PSS	CA	0.05	0.05−79	AA, UA, Glu, DOPAC	this work

Calibration of the Microelectrode. The calibration process was performed under a three-electrode configuration in a PBS solution. The chronoamperometry was applied under the potential of 0.2 V, and various concentrations of 10 μL DA solutions got added into PBS solution. The electrode current signal-to-noise (S/N) exceeded 3 upon adding a 50 nM DA solution, indicating the detection limit of the DA sensor was around 50 nM. Figure S3a displayed a typical DA channel calibration curve with the DA adding concentration from 1 to 30 μM. And the current response curve with the low DA concentration range (50 nM to 1 μM) was also shown in Figure S3b. All the calibration curves showed a good current response of DA. The corresponding calibration fitting curve was shown in Figure 6a, which exhibited a high linearity (R = 0.995) and high sensitivity of 30.561 pA/μM in the range from 50 nM to 79 μM. The proposed biochemical sensor was compared with other reported methods as shown in Table 1, which exhibited a more excellent performance in DA detection.

To investigate the precision for the proposed sensors, the chronoamperometry measurements were performed repetitively using the same modified electrodes, and the R.SD value less than 2% in sensitivity was obtained for the DA measurements (Table S1), which verified the superior reproducibility of the proposed biosensors. The stability for the modified electrodes was evaluated over a period of 20 days at 20 °C under a dry state.

https://doi.org/10.1021/acsabm.1c00172
ACS Appl. Bio Mater. 2021, 4, 4872−4884

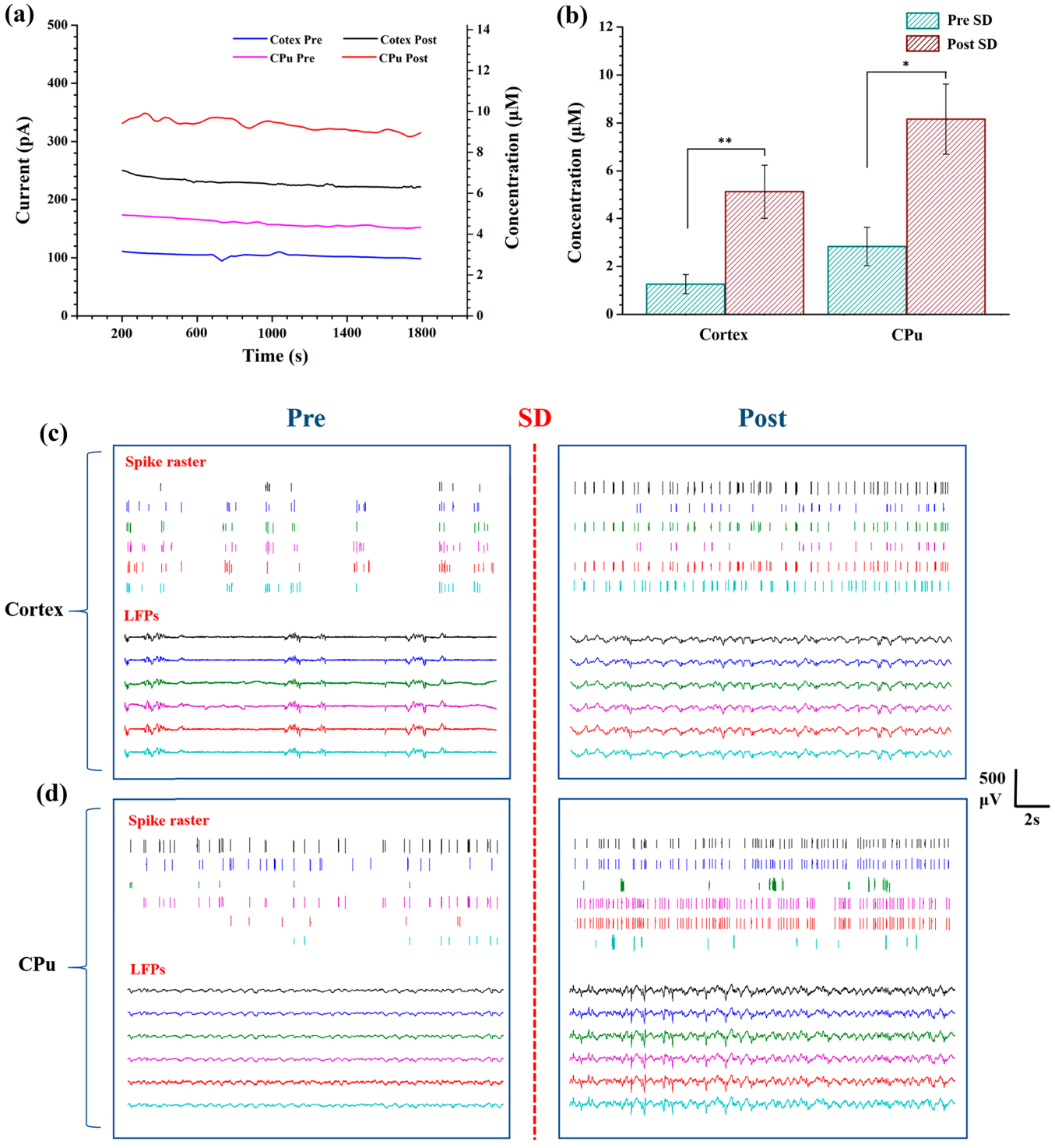

Figure 7. Recording of DA and neural spike activities in cortex and CPU before and after SD: (a) DA concentration changes in cortex and CPU before and after SD; (b) calculated mean concentration of DA in the cortex and CPU before and after SD; (c, d) neural spike firing and LFP recording in cortex and CPU before and after SD. Displayed recording channel = 6 for both the cortex and CPU. $n = 6$ rats, data are means ± SE, paired t test, * $p < 0.05$; ** $p < 0.01$.

The biosensors exhibited less than 20% loss in sensitivity (Figure S4), which verified its good film stability.

Ascorbic acid (AA), uric acid (UA), 3,4-dihydroxyphenylacetic acid (DOPAC), and glutamate (Glu) are molecules commonly found in the brain; the coexistence of these substances will affect the response current during DA measurement and impact the accuracy of the DA measurements. The oxidation potential of DA could significantly be reduced through PtNPt/MWCNT-PEDOT:PSS modification, distinguishing the detection of DA from other molecules. And the coated Nafion could further block the interference of anion. As can be seen from Figure 6b, DA, DOPAC, Glu, UA, and AA solutions of the same concentration (20 μM) were added in sequence to the PBS solution. The electrode showed good selectivity of DA against other molecules. Compared with DA response, the electrode showed almost no obvious response to the addition of DOPAC,

https://doi.org/10.1021/acsabm.1c00172
ACS Appl. Bio Mater. 2021, 4, 4872−4884

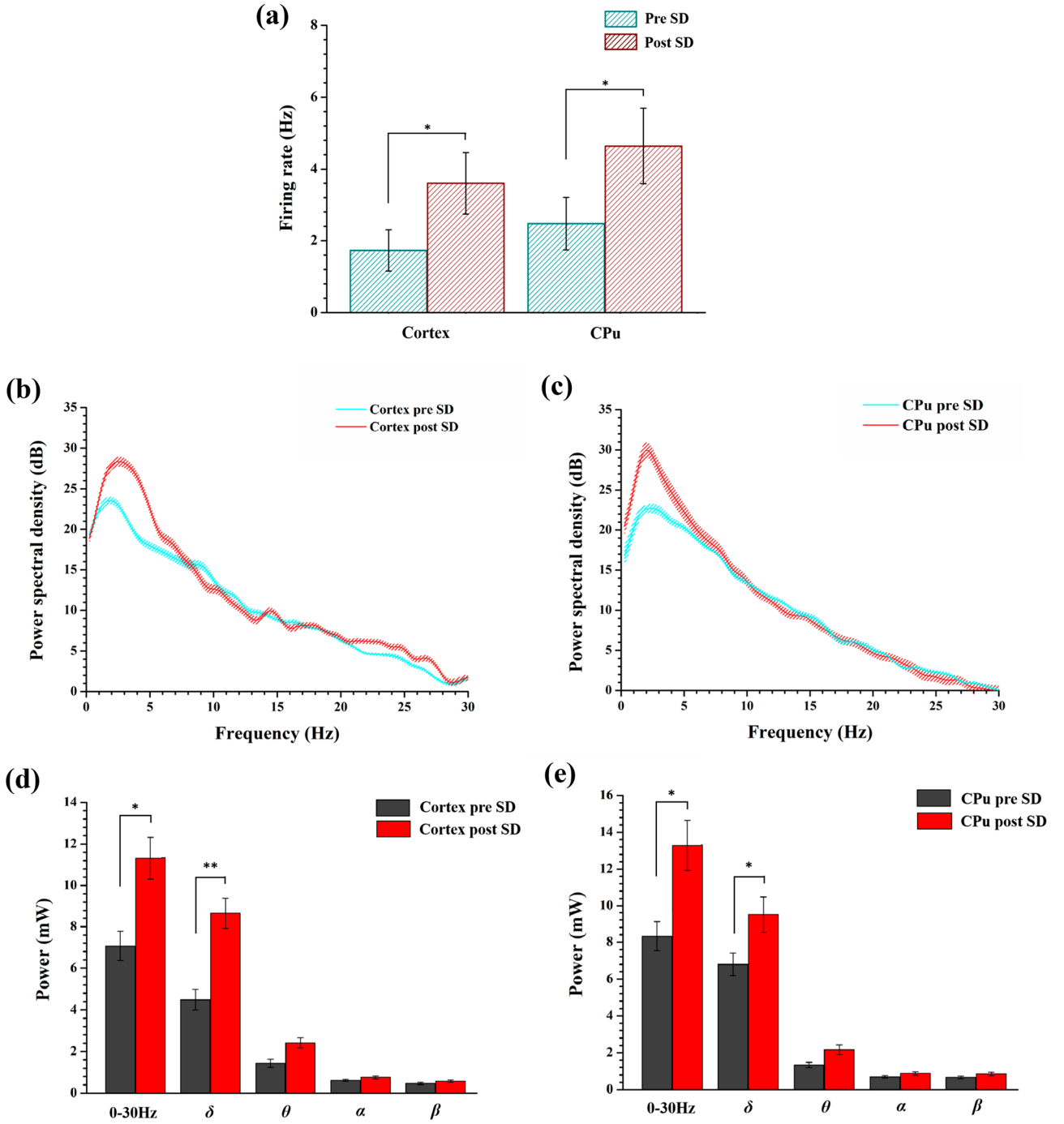

Figure 8. Changes of spike firing rate and LFP power in cortex and CPU before and after SD: (a) firing rate changes in cortex and CPU before and after SD; (b, c) LFP power spectral density under 30 Hz in cortex and CPU before and after SD; (d, e) LFP power calculated in cortex and CPU before and after SD. The power in the frequency of 0−30 Hz, δ, θ, α, and β band was calculated and compared, respectively. $n = 6$ rats, data are means ± SE, paired t test, * $p < 0.05$; ** $p < 0.01$.

Glu, UA, or AA. The calculated selectivity ratios for DA to DOPAC, Glu, UA, and AA were 95.8, 98.1, 95.7, and 93.9%, respectively (Figure 6c), which satisfied the requirements for the in vivo detection.

In Vivo Synchronous Detection of DA Levels and Neuronal Activities before and after SD. The MEAs were implanted into the rat brain and slowly moved to the cortex and CPU in sequence to record the dual-mode neural signals. The recording sites on the probe tips are closely contacted with the neurons in the target region, so the information exhibited in each channel could clearly reflect the signal it detected.

The DA concentration levels were recorded in the cortex and CPU before and after the sleep deprivation, as shown in Figure 7a. The displayed recording periods were from 200 to 1800 s. The concentration levels kept stable during the recording process, verifying the ability of the electrode to dynamically detect the neurochemical signals. It was noted that the DA concentrations after the sleep deprivation were significantly increased, both in cortex and CPU. And other electrochemical

https://doi.org/10.1021/acsabm.1c00172
ACS Appl. Bio Mater. 2021, 4, 4872−4884

channels during several experiments exhibited the similar change trends. The calculated mean variations of the DA concentration in the cortex and CPU before and after the SD were shown in Figure 7b. We found that the DA concentration in cortex increased from 1.262 to 5.12 μM, and the DA concentration in CPU increase from 2.833 to 8.16 μM.

The neuronal spike activities were recorded concurrently with the DA measurements, and the real-time neural spike firings and local field potentials (LFPs) of six different channels in cortex and CPU before and after the SD were shown in Figure 7c, 7d. The period of each recording was in a duration of 20s, and all these cooperated multiple signals could perfectly reflect the neuronal activities. As can be seen, before the sleep deprivation, the spikes in both cortex and CPU showed a relatively slow firing pattern. And brief cease of spike firing would occasionally occur during the recording. Significantly, the spike firing in both brain regions became tight and more fierce after SD, accompanied by a much frequent and fierce fluctuation of LFPs. This indicated that sleep deprivation enhanced the neuronal activity in cortex and striatum (CPU), inducing a state of hyper-excitability in neurons.

Effect of SD on Spike Firing Rate and LFP Power. The changes in spike firing rate were calculated and compared in Figure 8a, the spike firing in both cortex and CPU increased significantly after SD. The spike firing rate in cortex was 1.731 Hz before the sleep deprivation and increased by 107.97% to 3.6 Hz after sleep deprivation. In the CPU, the spike firing rate was 2.473 Hz before the sleep deprivation and increased by 87.62% to 4.64 Hz after sleep deprivation.

The local field potential (LFP) is a measure of brain activity that reflects the highly dynamic flow of information across neural network. Contrary to the traditional EEG recordings, it shows the electrical information generated by local populations of neurons and could act as the supplement of action potential recordings. In this study, the power spectral density (PSD) were applied on the LFPs to get the knowledge of their features in frequency domain, and the Fast Fourier Transformation (FFT) algorithm was used to produce the power spectral density (PSD) of the LFPs in frequencies ranging from 0 to 30 Hz. As shown in Figure 8b, 8c, the PSD of LFPs in both cortex and CPU got elevated after sleep deprivation and the increase were observed to be mainly concentrated in the low frequency band. Figure 8d, e showed the mean gross power of LFPs in cortex and CPU under 30 Hz. The LFP power of delta, theta, alpha and beta band before and after SD got calculated and compared, respectively. And we found that the increase of power in delta and theta activities was significant in both cortex and CPU. However, no significant increase in alpha and beta waves was observed after SD. The results above indicated that the SD induced a significant increase of LFPs in slow waves, mainly the delta and theta band in both the cortex and CPU.

Correlation between the Neural Activity Changes and Sleep Deprivation. Dopamine is sometimes called the "pleasure neurotransmitter" because of its role in so many human behaviors.[49] Drugs that increase dopamine levels tend to increase wakefulness, and the patients with the depletion of dopamine in striatum usually feel drowsy during the daytime.[50] It was assumed that greater fatigue would produce greater DA increases, and the increase of dopamine after SD in this study may serve to maintain the state of arousal as the drive to sleep increases.

Neurons communicate via both electrophysiological signals and neurochemical signals. These two kinds of signals are highly interconnected. Once an action potential has reached the axon terminal of one neuron, the neuron can release the neurotransmitters. And the released neurotransmitters can in turn cause a rapid, temporary change in the membrane potential of the adjacent neuron to initiate an action potential in that neuron. In this way, the signal transduction can be realized from one neuron to another. However, only few researchers have focused on the concurrent changes of certain brain neurotransmitters and electrophysiological changes after sleep deprivation. Importantly, the present data revealed that the neurotransmitter dopamine release and the electrophysiological activities in both the cortex and CPU have increased after 72 h of SD, and the cortex was more severely influenced by SD than the CPU. In the cortex, the extent of DA change was not only larger than that in the CPU but also accompanied by a more significant elevation in spike firing. This evidence may indicate that the hyper-excitability state in neurons after SD is modulated by the increased dopamine release.

In addition, slow wave activity (SWA) has been proposed as the marker of neuronal synchronization, which reflects changes in synaptic efficacy across the sleep−wake cycle.[51,52] They increase with the accumulation of the preceding wake and decrease along with the NREM sleep. As shown from LFP power data obtained after 72 h of sleep SD, the activity of LFP in slow waves has been significantly increased in both cortex and CPU, which further reflects the enhanced neuronal synchronization. We may conclude that the elevated dopamine levels in both the cortex and CPU are correlated with the initiation of cerebral slow-wave rhythm that can be measured from both the cortical and striatal structures, and consequently give rise to a state of forced arousal.

All in all, after 72 h of sleep deprivation, the neural detecting data of the present study showed a state of hyper-excitability of neurons mediated by the increase in the waking-promoted dopamine neurotransmitters and was supported by the LFP power being changed toward an increase in slow wave activity. All these changes might partially reflect the mechanism by which the sleep deprived brain counterparts the effects of sleepiness and assists the sleep deprived individuals to stay alert with the accumulated sleep pressure. Numerous studies have shown that both total and partial sleep deprivation could induce much degradation in cognitive performance, such as the impairments in working memory and attention.[53,54] From this point, even the increase in DA could help improve the motor behavior and keep the rats awake, onto which the much degraded performances due to the correlated and greater adverse effects brought by SD are superimposed.

CONCLUSION

In this work, we designed and fabricated an implantable MEA for the synchronous detection of neurotransmitter dopamine and neuronal activities in the cortex and CPU of rats before and after the sleep deprivation. The microelectrodes were modified with PtNPt/MWCNT-PEDOT:PSS nanocomposites, which exhibits high conductivity, fast electron transfer, and high porosity properties. The sensitivity, selectivity and performance of the proposed biosensor were evaluated, which showed the good electrocatalytic behavior toward electrochemical oxidation of dopamine.

The study of sleep deprivation is important to explain the mechanism of sleep and wakefulness. The in vivo neural detection indicated the capabilities of the modified MEA to dynamically record changes of neurotransmitters and neuro-

https://doi.org/10.1021/acsabm.1c00172
ACS Appl. Bio Mater. 2021, 4, 4872−4884

physiology in multiple nucleus of rat brain. The results showed that the dopamine in cortex and CPU has significantly increased after 72 h sleep deprivation, and the neuronal firing rates have been elevated at the same time. And the analysis of LFP power revealed that the sleep deprivation has induced the power increase under the frequency of 30 Hz, which was manifested in slow wave activities including delta and theta band. It may be concluded that increased neural excitability and dopamine release after sleep deprivation might be the innate adaptive reaction of the brain to help reverse the effects of sleepiness and keep the individual awake. However, this adaption is clearly insufficient to counteract the behavioral and physiological impairments induced by sleep deprivation. This study may provide some insights into the protective measures against extreme conditions like aerospace environments, where the states of sleep deprivation and forced wakefulness are commonplace among the astronauts.

■ ASSOCIATED CONTENT

Supporting Information

The Supporting Information is available free of charge at https://pubs.acs.org/doi/10.1021/acsabm.1c00172.

Additional description about the MEA design, implantation of MEA into rat brain, the calibration of DA electrodes by adding DA solutions of different concentrations in PBS, and the exhibition of microelectrode performance in terms of repeatability and stability (PDF)

■ AUTHOR INFORMATION

Corresponding Authors

Xinxia Cai − *State Key Laboratory of Transducer Technology, Aerospace Information Research Institute, Chinese Academy of Sciences, Beijing 100120, China; University of Chinese Academy of Sciences, Beijing 100042, China;* orcid.org/0000-0001-5997-7252; Email: xxcai@mail.ie.ac.cn

Lina Qu − *State Key Laboratory of Space Medicine Fundamentals and Application, China Astronaut Research and Training Center, Beijing 100094, China*; Email: linaqu@263.net

Authors

Zeying Lu − *State Key Laboratory of Transducer Technology, Aerospace Information Research Institute, Chinese Academy of Sciences, Beijing 100120, China; University of Chinese Academy of Sciences, Beijing 100042, China*

Shengwei Xu − *State Key Laboratory of Transducer Technology, Aerospace Information Research Institute, Chinese Academy of Sciences, Beijing 100120, China; University of Chinese Academy of Sciences, Beijing 100042, China*

Hao Wang − *State Key Laboratory of Transducer Technology, Aerospace Information Research Institute, Chinese Academy of Sciences, Beijing 100120, China; University of Chinese Academy of Sciences, Beijing 100042, China*

Enhui He − *State Key Laboratory of Transducer Technology, Aerospace Information Research Institute, Chinese Academy of Sciences, Beijing 100120, China; University of Chinese Academy of Sciences, Beijing 100042, China*

Juntao Liu − *State Key Laboratory of Transducer Technology, Aerospace Information Research Institute, Chinese Academy of Sciences, Beijing 100120, China; University of Chinese Academy of Sciences, Beijing 100042, China*

Yuchuan Dai − *State Key Laboratory of Transducer Technology, Aerospace Information Research Institute, Chinese Academy of Sciences, Beijing 100120, China; University of Chinese Academy of Sciences, Beijing 100042, China*

Jingyu Xie − *State Key Laboratory of Transducer Technology, Aerospace Information Research Institute, Chinese Academy of Sciences, Beijing 100120, China; University of Chinese Academy of Sciences, Beijing 100042, China*

Yilin Song − *State Key Laboratory of Transducer Technology, Aerospace Information Research Institute, Chinese Academy of Sciences, Beijing 100120, China; University of Chinese Academy of Sciences, Beijing 100042, China*

Yun Wang − *State Key Laboratory of Transducer Technology, Aerospace Information Research Institute, Chinese Academy of Sciences, Beijing 100120, China; University of Chinese Academy of Sciences, Beijing 100042, China*

Yiding Wang − *State Key Laboratory of Transducer Technology, Aerospace Information Research Institute, Chinese Academy of Sciences, Beijing 100120, China; University of Chinese Academy of Sciences, Beijing 100042, China*

Complete contact information is available at: https://pubs.acs.org/10.1021/acsabm.1c00172

Author Contributions

Z.L. and H.W. designed the research approach and experiments. Z.L. and J.X. designed and fabricated the probes. Z.L. and H.W. conducted the experiments including animal surgery and data recording. Z.L., S.X., and Y.D. analyzed the recording signals. Z.L. wrote the manuscript. S.X. reviewed the manuscript.

Funding

This research was sponsored by the National Key R&D Program of China (2017YFA0205902), the National Natural Science Foundation of China (61960206012, 61975206, 61971400, 61973292, 61775216, 61771452), State Key Lab of Space Medicine Fundamentals and Application grants (SMFA19K05).

Notes

The authors declare no competing financial interest.

■ REFERENCES

(1) Riganello, F.; Prada, V.; Soddu, A.; di Perri, C.; Sannita, W. G. Circadian Rhythms and Measures of CNS/Autonomic Interaction. *Int. J. Environ. Res. Public Health* **2019**, *16* (13), 2336.

(2) Volkow, N. D.; Tomasi, D.; Wang, G. J.; Telang, F.; Fowler, J. S.; Logan, J.; Benveniste, H.; Kim, R.; Thanos, P. K.; Ferré, S. Evidence that sleep deprivation downregulates dopamine D2R in ventral striatum in the human brain. *J. Neurosci.* **2012**, *32* (19), 6711−7.

(3) Potter, G. D. M.; Skene, D. J.; Arendt, J.; Cade, J. E.; Grant, P. J.; Hardie, L. J. Circadian Rhythm and Sleep Disruption: Causes, Metabolic Consequences, and Countermeasures. *Endocr. Rev.* **2016**, *37* (6), 584−608.

(4) Sigurdson, K.; Ayas, N. T. The public health and safety consequences of sleep disorders. *Can. J. Physiol. Pharmacol.* **2007**, *85* (1), 179−83.

(5) Nasim, M.; Saade, M.; AlBuhairan, F. Sleep deprivation: prevalence and associated factors among adolescents in Saudi Arabia. *Sleep Medicine* **2019**, *53*, 165−171.

(6) Jean-Louis, G.; Williams, N. J.; Sarpong, D.; Pandey, A.; Youngstedt, S.; Zizi, F.; Ogedegbe, G. Associations between inadequate sleep and obesity in the US adult population: analysis of the national health interview survey (1977−2009). *BMC Public Health* **2014**, *14* (1), 290.

(7) Muzur, A.; Pace-Schott, E. F.; Hobson, J. A. The prefrontal cortex in sleep. Trends in Cognitive. *Trends Cognit. Sci.* **2002**, *6* (11), 475−481.

(8) Brown, R. E.; Basheer, R.; McKenna, J. T.; Strecker, R. E.; McCarley, R. W. Control of sleep and wakefulness. *Physiol. Rev.* **2012**, *92* (3), 1087−1187.
(9) Yuan, X. S.; Wang, L.; Dong, H.; Qu, W. M.; Yang, S. R.; Cherasse, Y.; Lazarus, M.; Schiffmann, S. N.; d'Exaerde, A. K.; Li, R. X.; Huang, Z. L. Striatal adenosine A(2A) receptor neurons control active-period sleep via parvalbumin neurons in external globus pallidus. *eLife* **2017**, *6*, e29055.
(10) Schwartz, J. R. L.; Roth, T. Neurophysiology of sleep and wakefulness: basic science and clinical implications. *Curr. Neuropharmacol* **2008**, *6* (4), 367−378.
(11) Watson, C. J.; Baghdoyan, H. A.; Lydic, R. Neuropharmacology of Sleep and Wakefulness. *Sleep Med. Clin* **2010**, *5* (4), 513−528.
(12) Palmiter, R. D. Is dopamine a physiologically relevant mediator of feeding behavior? *Trends Neurosci.* **2007**, *30* (8), 375−81.
(13) Berke, J. D. What does dopamine mean? *Nat. Neurosci.* **2018**, *21* (6), 787−793.
(14) Lazarus, M.; Huang, Z. L.; Lu, J.; Urade, Y.; Chen, J. F. How do the basal ganglia regulate sleep−wake behavior? *Trends Neurosci.* **2012**, *35* (12), 723−32.
(15) Lazarus, M.; Shen, H. Y.; Cherasse, Y.; Qu, W. M.; Huang, Z. L.; Bass, C. E.; Winsky-Sommerer, R.; Semba, K.; Fredholm, B. B.; Boison, D.; Hayaishi, O.; Urade, Y.; Chen, J. F. Arousal effect of caffeine depends on adenosine A2A receptors in the shell of the nucleus accumbens. *J. Neurosci.* **2011**, *31* (27), 10067−75.
(16) Nishino, S.; Mao, J.; Sampathkumaran, R.; Shelton, J. Increased dopaminergic transmission mediates the wake-promoting effects of CNS stimulants. *Sleep Research Online: SRO* **1998**, *1* (1), 49−61.
(17) Dzirasa, K.; Ribeiro, S.; Costa, R.; Santos, L. M.; Lin, S. C.; Grosmark, A.; Sotnikova, T. D.; Gainetdinov, R. R.; Caron, M. G.; Nicolelis, M. A. Dopaminergic control of sleep−wake states. *J. Neurosci.* **2006**, *26* (41), 10577−89.
(18) Lu, J.; Jhou, T. C.; Saper, C. B. Identification of wake-active dopaminergic neurons in the ventral periaqueductal gray matter. *J. Neurosci.* **2006**, *26* (1), 193−202.
(19) Boutrel, B.; Koob, G. F. What keeps us awake: the neuropharmacology of stimulants and wakefulness-promoting medications. *Sleep* **2004**, *27* (6), 1181−94.
(20) Adler, C. H.; Thorpy, M. J. Sleep issues in Parkinson's disease. *Neurology* **2005**, *64* (12 suppl 3), S12.
(21) Kume, K.; Kume, S.; Park, S. K.; Hirsh, J.; Jackson, F. R. Dopamine is a regulator of arousal in the fruit fly. *J. Neurosci.* **2005**, *25* (32), 7377−84.
(22) Saylor, R. A.; Lunte, S. M. A review of microdialysis coupled to microchip electrophoresis for monitoring biological events. *J. Chromatogr A* **2015**, *1382*, 48−64.
(23) Nandi, P.; Lunte, S. M. Recent trends in microdialysis sampling integrated with conventional and microanalytical systems for monitoring biological events: a review. *Anal. Chim. Acta* **2009**, *651* (1), 1−14.
(24) Szostak, K. M.; Grand, L.; Constandinou, T. G. Neural Interfaces for Intracortical Recording: Requirements, Fabrication Methods, and Characteristics. *Front. Neurosci.* **2017**, *11*, 665−665.
(25) Meyyappan, M. Nano biosensors for neurochemical monitoring. *Nano Convergence* **2015**, *2* (1), 18.
(26) Abdel-Karim, R.; Reda, Y.; Abdel-Fattah, A. Review—Nanostructured Materials-Based Nanosensors. *J. Electrochem. Soc.* **2020**, *167* (3), No. 037554.
(27) Siriviriyanun, A.; Imae, T. Advantages of electrodes with dendrimer-protected platinum nanoparticles and carbon nanotubes for electrochemical methanol oxidation. *Phys. Chem. Chem. Phys.* **2013**, *15* (14), 4921−9.
(28) Yoon, H. Current Trends in Sensors Based on Conducting Polymer Nanomaterials. *Nanomaterials* **2013**, *3* (3), 524−549.
(29) Khan, M. Z. H.; Ahommed, M. S.; Daizy, M. Detection of xanthine in food samples with an electrochemical biosensor based on PEDOT:PSS and functionalized gold nanoparticles. *RSC Adv.* **2020**, *10* (59), 36147−36154.
(30) Atta, N. F.; Galal, A.; El-Ads, E. H. Gold nanoparticles-coated poly(3,4-ethylene-dioxythiophene) for the selective determination of sub-nano concentrations of dopamine in presence of sodium dodecyl sulfate. *Electrochim. Acta* **2012**, *69*, 102−111.
(31) Yang, X.; Feng, B.; He, X.; Li, F.; Ding, Y.; Fei, J. Carbon nanomaterial based electrochemical sensors for biogenic amines. *Microchim. Acta* **2013**, *180* (11), 935−956.
(32) Zhang, S.; Song, Y.; Wang, M.; Xiao, G.; Gao, F.; Li, Z.; Tao, G.; Zhuang, P.; Yue, F.; Chan, P.; Cai, X. Real-time simultaneous recording of electrophysiological activities and dopamine overflow in the deep brain nuclei of a non-human primate with Parkinson's disease using nano-based microelectrode arrays. *Microsystems & Nanoengineering* **2018**, *4* (1), 17070.
(33) Xiao, G.; Song, Y.; Zhang, Y.; Xing, Y.; Zhao, H.; Xie, J.; Xu, S.; Gao, F.; Wang, M.; Xing, G.; Cai, X. Microelectrode Arrays Modified with Nanocomposites for Monitoring Dopamine and Spike Firings under Deep Brain Stimulation in Rat Models of Parkinson's Disease. *ACS sensors* **2019**, *4* (8), 1992−2000.
(34) He, B.; Li, Q.; Jia, Y.; Zhao, L.; Xiao, F.; Lv, C.; Xu, H.; Chen, X.; Bi, K. A UFLC-MS/MS method for simultaneous quantitation of spinosin, mangiferin and ferulic acid in rat plasma: application to a comparative pharmacokinetic study in normal and insomnic rats. *J. Mass Spectrom.* **2012**, *47* (10), 1333−40.
(35) Corum, C. R.; Thurmond, J. B. Effects of PCPA and selective REM sleep deprivation on rotorod performance and open-field behavior in the rat. *Bull. Psychon. Soc.* **1978**, *11* (4), 251−254.
(36) Benavente, J. Electrochemical Impedance Spectroscopy as a Tool for Electrical and Structural Characterizations of Membranes in Contact with Electrolyte Solutions. In *Recent Advances in Multidisciplinary Applied Physics*; Méndez-Vilas, A., Ed.; Elsevier Science: Oxford, U.K., 2005; pp 463−471.
(37) Ali Karimi, M. Sensitive Electrochemical Detection of Dopamine, Uric and Ascorbic Acids Based on poly-(Dianix Yellow) Film Modified Electrode. *Int. J. Electrochem. Sci.* **2017**, *12*, 7089−7102.
(38) Yusoff, F.; Khing, N. T.; Chai, C. H.; Sang, L. P.; Muhamad, N. B. The electrochemical behavior of zinc oxide/reduced graphene oxide composite electrode in dopamine. *Malaysian Journal of Analytical Sciences* **2018**, *22* (2), 227−237.
(39) Zhang, S.; Song, Y.; Wang, M.; Zhang, Z.; Fan, X.; Song, X.; Zhuang, P.; Yue, F.; Chan, P.; Cai, X. A silicon based implantable microelectrode array for electrophysiological and dopamine recording from cortex to striatum in the non-human primate brain. *Biosens. Bioelectron.* **2016**, *85*, 53−61.
(40) Harley, C. C.; Rooney, A. D.; Breslin, C. B. The selective detection of dopamine at a polypyrrole film doped with sulfonated β-cyclodextrins. *Sens. Actuators, B* **2010**, *150* (2), 498−504.
(41) Aparna, T. K.; Sivasubramanian, R.; Dar, M. A. One-pot synthesis of Au-Cu2O/rGO nanocomposite based electrochemical sensor for selective and simultaneous detection of dopamine and uric acid. *J. Alloys Compd.* **2018**, *741*, 1130−1141.
(42) Zhao, J.; Zhang, W.; Sherrell, P.; Razal, J. M.; Huang, X. F.; Minett, A. I.; Chen, J. Carbon Nanotube Nanoweb−Bioelectrode for Highly Selective Dopamine Sensing. *ACS Appl. Mater. Interfaces* **2012**, *4* (1), 44.
(43) Liu, S.-Q.; Sun, W.-H.; Hu, F.-T. Graphene nano sheet-fabricated electrochemical sensor for the determination of dopamine in the presence of ascorbic acid using cetyltrimethylammonium bromide as the discriminating agent. *Sens. Actuators, B* **2012**, *173*, 497−504.
(44) Meng, L.; Turner, A. P. F.; Mak, W. C. Modulating Electrode Kinetics for Discrimination of Dopamine by a PEDOT:COOH Interface Doped with Negatively Charged Tricarboxylate. *ACS Appl. Mater. Interfaces* **2019**, *11* (37), 34497−34506.
(45) Reddy, S.; Xiao, Q.; Liu, H.; Li, C.; Chen, S.; Wang, C.; Chiu, K.; Chen, N.; Tu, Y.; Ramakrishna, S.; He, L. Bionanotube/poly(3,4-ethylenedioxythiophene) nanohybrid as an electrode for neural interface and dopamine sensor. *ACS Appl. Mater. Interfaces* **2019**, *11* (20), 18254−18267.
(46) Choe, J. E.; Ahmed, M. S.; Jeon, S. Trouble Free Dopamine Sensing by Palladium Nanoparticles Fabricated Poly(3,4-ethylenediox-

https://doi.org/10.1021/acsabm.1c00172
ACS Appl. Bio Mater. 2021, 4, 4872−4884

ythiophene) Functionalized Graphene. *J. Electrochem. Soc.* **2016**, *163* (3), B113−B118.
(47) Xu, G.; Jarjes, Z. A.; Desprez, V.; Kilmartin, P. A.; Travas-Sejdic, J. Sensitive, selective, disposable electrochemical dopamine sensor. based on PEDOT-modified laser scribed graphene. *Biosens. Bioelectron.* **2018**, *107*, 184−191.
(48) Liu, K.; Pang, H.; Zhang, J.; Huang, H.; Liu, Q.; Chu, Y. Synthesis and characterization of a highly stable poly (3,4-ethylenedioxythiophene)-gold nanoparticles composite film and its application to electrochemical dopamine sensors. *RSC Adv.* **2014**, *4* (17), 8415−8420.
(49) Berridge, K. C.; Kringelbach, M. L. Pleasure systems in the brain. *Neuron* **2015**, *86* (3), 646−664.
(50) Dong, H.; Wang, J.; Yang, Y. F.; Shen, Y.; Qu, W. M.; Huang, Z. L. Dorsal Striatum Dopamine Levels Fluctuate Across the Sleep−Wake Cycle and Respond to Salient Stimuli in Mice. *Front. Neurosci.* **2019**, *13*, 242.
(51) Esser, S. K.; Hill, S. L.; Tononi, G. Sleep homeostasis and cortical synchronization: I. Modeling the effects of synaptic strength on sleep slow waves. *Sleep* **2007**, *30* (12), 1617−1630.
(52) Vyazovskiy, V. V.; Olcese, U.; Lazimy, Y. M.; Faraguna, U.; Esser, S. K.; Williams, J. C.; Cirelli, C.; Tononi, G. Cortical firing and sleep homeostasis. *Neuron* **2009**, *63* (6), 865−878.
(53) Alhola, P.; Polo-Kantola, P. Sleep deprivation: Impact on cognitive performance. *Neuropsychiatr Dis Treat* **2007**, *3* (5), 553−567.
(54) Killgore, W. D. Effects of sleep deprivation on cognition. *Prog. Brain Res.* **2010**, *185*, 105−29.

https://doi.org/10.1021/acsabm.1c00172
ACS Appl. Bio Mater. 2021, 4, 4872−4884